Journal of Catalysis **192,** 54–63 (2000)
doi:10.1006/jcat.2000.2814, available online at http://www.idealibrary.com on IDEAL®

Mechanistic Study of the Selective Catalytic Reduction of Nitric Oxide with Methane over Yttrium Oxide

Mark D. Fokema and Jackie Y. Ying[1]

Department of Chemical Engineering, Massachusetts Institute of Technology, Cambridge, Massachusetts 02139

Received August 10, 1999; revised January 5, 2000; accepted January 6, 2000

The catalytic activity of nanocrystalline Group IIIB metal oxides for the reduction of nitric oxide with methane was shown to be comparable to that of Co-ZSM-5. The mechanism of selective catalytic reduction of nitric oxide with methane in excess oxygen was examined over nanocrystalline yttrium oxide. A series of heterogeneous and homogeneous reaction steps was proposed to account for the observed trends in catalytic properties. Methyl radicals generated at the catalyst surface desorb into the gas phase, where they react with nitric oxide to form nitrosomethane. Nitrosomethane then decomposes in a series of homogeneous and heterogeneous reactions to produce nitrogen and nitrous oxide. Evidence for gas-phase reaction of methyl radicals with nitric oxide was found in the adsorption studies of nitric oxide on yttrium oxide, the presence of ethane and ethene in the reactor effluent, catalytic studies involving nitrosomethane and nitromethane, as well as the successful prediction of methane selectivities based on a homogeneous reaction mechanism for methyl radical consumption. The proposed pathway for nitrogen production was supported by the observation of hydrogen cyanide under certain operating conditions, as well as adsorbed NCO species detected by infrared spectroscopy.

Key Words: **selective catalytic reduction; nitrogen monoxide; methane; rare earth oxide; mechanism.**

INTRODUCTION

The catalytic reduction of nitrogen oxides (NO_x) to N_2 is one of the best available control technologies for reducing NO_x emissions from stationary and mobile sources (1). Ammonia and hydrocarbons have commonly been studied as selective reducing agents in this NO_x emission control technique (2), but in the past decade the use of methane as a reducing agent has drawn a great deal of attention (3). Methane offers the benefits of low cost and wide availability compared to other hydrocarbons, and it is much less corrosive than ammonia. The use of methane thus offers the opportunity for significantly reduced capital and operating costs compared to other reducing agents.

Many materials have been shown to catalytically reduce NO_x in the presence of methane, but only a few materials have been shown to be true "selective" catalytic reduction (SCR) catalysts, with the ability to reduce NO_x in the presence of a large excess of oxygen. The selective catalysts include metal-exchanged zeolites such as Co-ZSM-5 (4–6), lanthanide oxides (7, 8), Group IIA metal oxides (9), Group IIIB metal oxides (10), SnO_2 (11), Ga/sulfated-ZrO_2 (12), and Ga/Al_2O_3 (13). Many studies have been performed on the Co–zeolite system in an effort to identify the mechanism of NO_x reduction by methane over the zeolitic class of catalysts. Catalytic (14–17), infrared (18, 19), and XPS (20) studies have revealed many details of the mechanism and have offered insights into the development of better zeolitic catalysts for the SCR of NO_x with methane.

Although Group IIA, Group IIIB, and lanthanide oxide catalysts are not as active as some zeolitic catalysts for the selective catalytic reduction of NO_x with methane, these materials do exhibit significantly better hydrothermal and high-temperature stability than many of the zeolitic systems that have been studied (10, 21). Surprisingly, only a few reports have been made regarding the mechanism of NO_x reduction over these nonzeolitic catalysts. Vannice *et al.* performed a kinetic analysis employing Langmuir–Hinshelwood-type elementary reactions for pure and strontium-doped lanthanum oxide catalysts (22). Based on known homogeneous elementary reactions, they proposed that adsorbed CH_4 and NO_2 species react to produce adsorbed CH_3. The methyl species then react with adsorbed NO_x to produce HCN, which further reacts to produce CN and NCO. The surface NCO species then react with adsorbed NO to produce N_2O, which in turn is decomposed on the surface to produce N_2.

It has been suggested that the formation of methyl radicals is the first step in the selective catalytic reduction of NO_x to N_2 with CH_4 (8, 22, 23). Group IIIB metal oxides and lanthanide oxides are known to be effective catalysts for the oxidative coupling of methane (24, 25), so formation of methyl radical species under SCR conditions would not be unexpected. Xie *et al.* have detected methyl radicals emanating from the surface of Sr/La_2O_3 upon exposure of the catalyst to a gas stream containing a 10 : 10 : 1 mixture of $CH_4 : NO : O_2$ reactants at 735°C and 0.5 Torr (23),

[1] To whom correspondence should be addressed.

0021-9517/00 $35.00

indicating the possibility of gas-phase reactions playing a critical role in the reduction of NO_x over these catalysts. Unfortunately, the conditions examined are far removed from actual SCR conditions (i.e., excess oxygen, atmospheric pressure). Two important questions that need to be answered regarding the SCR mechanism over these nonzeolitic catalysts are: (i) whether reactions of methyl radicals with NO_x in excess O_2 at atmospheric pressure occur in the gas phase or on the surface of the catalyst, and (ii) whether this reaction involves coupling of methyl radicals with NO species to produce CH_3NO, or with NO_2 species to form CH_3NO_2.

This paper reports on a series of studies aimed at gaining direct evidence of the mechanism for the selective catalytic reduction of NO_x with methane over yttrium oxide. Nanocrystalline yttrium oxide catalyst was the focus of this study, as yttrium oxide has a high selectivity and activity for the SCR of NO_x with methane. However, the mechanism elucidated in this study likely also applies to other Group IIIB metal oxides (10) and many rare earth oxides (26).

EXPERIMENTAL

Nanocrystalline yttrium oxide catalysts were prepared using a chemical precipitation technique, in which aqueous solutions of yttrium nitrate (Alfa Aesar, 99.9%) and tetraethylammonium hydroxide (Aldrich) were mixed and aged for 24 h (27). After washing the precipitate with ethanol, the material was air-dried and then oven-dried at 120°C. The powder was calcined in flowing oxygen for 4 h to convert the yttrium hydroxynitrate precipitate to pure yttrium oxide. Catalyst surface area was determined by nitrogen adsorption using a 5-point BET (Brunauer–Emmett–Teller) method on a Micromeritics ASAP 2000 instrument. Phase identification was achieved with powder X-ray diffraction (XRD) using a Siemens D5000 diffractometer (45 kV, 40 mA, Cu $K\alpha$). Scherrer's analysis of the X-ray peak broadening of the Y_2O_3 (222) reflection was employed to determine crystallite size. XRD measurements of sintered, polycrystalline Y_2O_3 were used to correct for instrumental line broadening.

Co-ZSM-5 was prepared by ion-exchanging Na-ZSM-5 (W.R. Grace, Si/Al = 14) three times with aqueous cobalt acetate at 80°C. The final cobalt loading as determined by elemental analysis was 3.4 wt%, which corresponds to an exchange level of 106%.

Catalytic activity measurements were performed at atmospheric pressure under steady-state reaction conditions, in a 1/4-in.-O.D. quartz tube catalytic reactor with the catalyst supported on a porous quartz frit. Type K thermocouples were located above and below the catalyst bed, and were used in conjunction with an Omega temperature controller and a Lindberg tube furnace to maintain the catalyst within 2°C of the desired operating temperature. High-purity gases (BOC) (He, 10.0% O_2–He, 1.48% NO–He, and 1.99% CH_4–He) were metered into the top of the quartz reactor with four independent MKS mass flow controllers. The reactor effluent was analyzed with a Perkin–Elmer Autosystem gas chromatograph equipped with a 10-ft × 1/8-in.-O.D. molecular sieve 5A column and a 12-ft × 1/8-in.-O.D. Porapak Q column. This allowed oxygen, nitrogen, nitrous oxide, methane, carbon dioxide, carbon monoxide, ethane, and ethene in the reactor effluent to be separated and quantified. Hydrogen and hydrogen cyanide could also be detected but were not quantified. Carbon balances to within 2.5% were always obtained. Blank experiments with nitric oxide, methane, and oxygen indicated that homogeneous and wall-catalyzed reactions were not significant in any of our experiments.

The nitric oxide conversion is based on the nitrogen formation, and the methane conversion is based on the methane consumption. The methane selectivity is defined as the ratio of the amount of methane reacted with nitric oxide to the total amount of methane consumed (i.e., (rate of formation of N_2 and N_2O)/(rate of CH_4 consumption), similar to α as defined by Li and Armor (6)). The selective reaction is assumed to involve the reaction of two molecules of nitric oxide per molecule of methane (6).

Diffuse reflectance infrared Fourier-transform (DRIFT) spectra were collected using a Harrick HVC-DR2 diffuse reflectance cell on a Bio-Rad FTS-60A spectrometer. Following pretreatment in 5% O_2–He for 1 h at the reaction temperature, the catalyst was exposed to a gas mixture containing 1% NO, 10% CH_4, and 10% O_2. Each spectrum consisted of 128 scans that were taken at a resolution of 2 cm^{-1} in the presence of the reaction gases. The spectrum of the catalyst in 5% O_2–He at the same temperature was used as a reference spectrum.

Samples for temperature-programmed desorption (TPD) of NO_x were pretreated in 5% O_2–He at 800°C for 6 h to remove surface carbonate species. Following cooling to room temperature, samples were exposed to 4000 ppm NO and 8000 ppm O_2 overnight. Desorption of adsorbed species was performed at a ramp rate of 10°C/min in flowing helium at atmospheric pressure, and was measured using a Thermoelectron Series 10 Chemiluminescent NO_x analyzer.

Thermal gravimetric analysis (TGA) was performed with a Perkin–Elmer TGA7. The sample was pretreated in 8000 ppm O_2–He for 6 h at 800°C. Adsorption of NO_x was quantified by measuring the weight change of the sample upon switching of the gas stream from 8000 ppm O_2 in He to 4000 ppm NO and 8000 ppm O_2 in He, and then back to 8000 ppm O_2 in He. Differences in the buoyancy of the sample in different atmospheres were accounted for at each temperature.

Nitromethane was introduced into the reactor by passing He through a gas bubbler containing CH_3NO_2 (Aldrich) at room temperature. CH_3NO dimer was synthesized by the

TABLE 1

BET Surface Area and XRD Crystallite Size of Y_2O_3 Catalysts

Catalyst	Calcination temperature (°C)	Surface area (m^2/g)	Crystallite size (nm)
Y600	600	106	9
Y800	800	52	17
Y1000	1000	22	39

photolysis of *tert*-butyl nitrate (Aldrich) (28). Five milliliters of *tert*-butyl nitrate at 40°C were irradiated for 8 h with a 200-W medium-pressure UV lamp (Canrad-Hanovia). The resulting crystalline deposit (*trans*-nitrosomethane dimer) was recrystallized from ethanol. Mass spectroscopic analysis gave intense peaks at m/e of 45, 30, and 15. CH_3NO was introduced into the catalytic reactor by gently warming a flask containing 500 mg of the dimer to 140°C and allowing the vapor to diffuse into a stream of He flowing to the reactor.

RESULTS AND DISCUSSION

The three different yttrium oxide catalysts used in this study were prepared by calcination of a high surface area precipitate to 600, 800, and 1000°C. X-ray diffraction revealed that all catalysts were cubic Y_2O_3 (JCPDS No. 41-1105). The BET surface areas and XRD crystallite sizes of the catalysts are presented in Table 1.

The NO_x reduction activity, CH_4 conversion, and selectivity of Y800 and Co-ZSM-5 in excess O_2 are shown in Fig. 1. The activity window for Y800 is approximately 100°C higher than that for Co-ZSM-5, but the two materials exhibit comparable maximum activities. The CH_4 selectivities of both materials decrease with increasing temperature, with the selectivity over Y800 greater than that over Co-ZSM-5 above 475°C. Both CH_3NO_2 (16, 17) and CH_3NO (29) have been proposed as possible intermediates in the SCR of NO_x with CH_4 over Co-ZSM-5. Similarities in the NO_x reduction and methane selectivity profiles for Y800 and Co-ZSM-5 suggest that these intermediates may also play an important role in the reduction of NO_x over Y_2O_3.

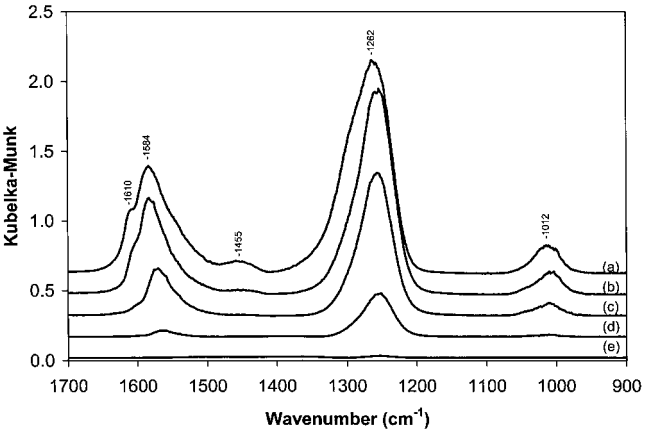

FIG. 2. DRIFT spectra of Y600 exposed to NO and O_2 at (a) 100, (b) 200, (c) 300, (d) 400, and (e) 500°C.

The adsorption of NO and O_2 on Y_2O_3 was examined via *in situ* DRIFT studies. Spectra of Y600 in the presence of 4000 ppm NO and 8000 ppm O_2 at 100, 200, 300, 400, and 500°C are shown in Fig. 2. The spectrum at 100°C exhibits peaks at 1610, 1584, 1455, 1262, and 1012 cm^{-1}; while at 400°C, the only peaks observed are at 1565, 1253, and 1010 cm^{-1}. The band at 1610 cm^{-1} can be attributed to gas-phase NO_2, and it disappears as the temperature is raised due to the shift in the NO–NO_2 equilibrium to NO at elevated temperatures (30, 31). The three strongest bands in the spectrum at 400°C can be assigned to vibrational modes

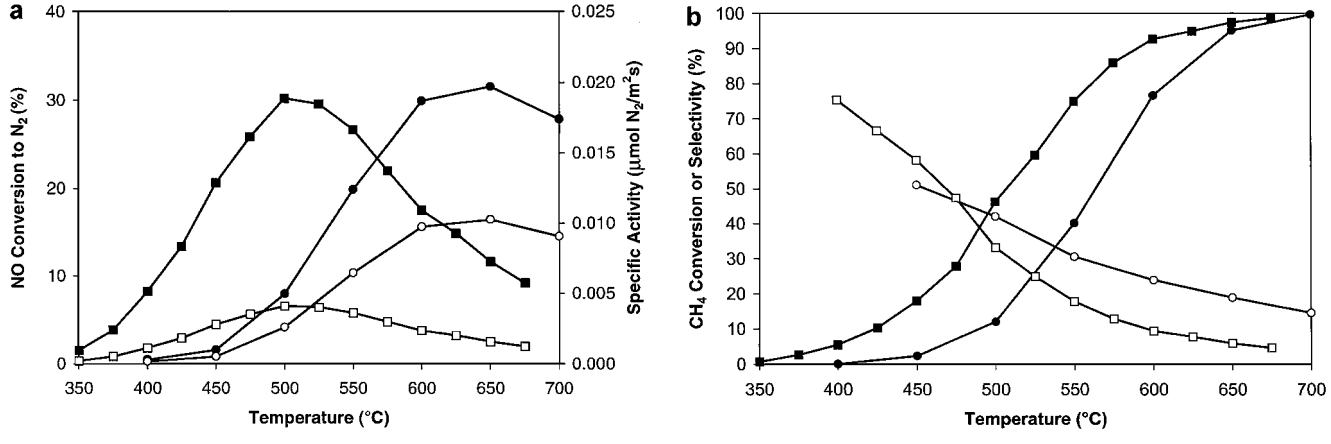

FIG. 1. (a) NO conversion (filled symbols) and specific rate of N_2 formation (open symbols) of (circles) Y800 and (squares) Co-ZSM-5. (b) CH_4 conversion (filled symbols) and CH_4 selectivity (open symbols) of (circles) Y800 and (squares) Co-ZSM-5. The reaction was run at a space velocity of 60000 h^{-1} with 4000 ppm NO, 4000 ppm CH_4, and 4% O_2.

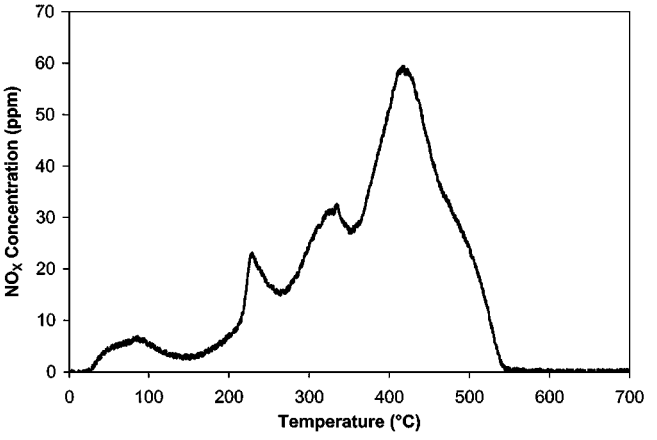

FIG. 3. Temperature-programmed desorption of NO_x from Y1000 following exposure to 4000 ppm NO and 8000 ppm O_2 at 25°C.

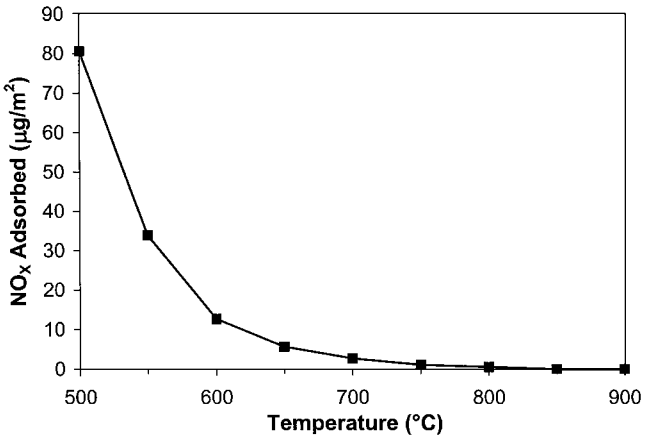

FIG. 4. Reversible adsorption of NO_x on Y1000 as determined by TGA.

of a unidentate nitrate group, with a NO_2 symmetric stretch at 1565 cm^{-1}, a NO_2 asymmetric stretch at 1253 cm^{-1}, and a N–O stretch at 1010 cm^{-1} (32, 33). The greater breadth of the bands at lower temperature, along with a slight shift to higher wavenumber may be associated with the presence of a chelated bidentate nitrate at lower temperature (32). We have assigned the peak at 1455 cm^{-1} to an N=O stretch from a nitrite group, with the corresponding N–O stretch ($\sim$1050 cm^{-1} (32)) obscured by the N–O stretch of the nitrate group. The following conclusions were drawn from this study: (i) the total amount of NO_x adsorbed on Y_2O_3 decreases with temperature, with the most significant decrease occurring between 300 and 400°C; (ii) nitrite and chelated bidentate nitrate groups that are stable at low temperature decompose by 300°C; and (iii) the only surface species stable between 300 and 500°C is the unidentate nitrate species.

Temperature-programmed desorption of NO_x from Y1000, shown in Fig. 3, illustrates that there are no NO_x species irreversibly adsorbed on the surface of Y_2O_3 above 540°C. Given the inherent shift of features to higher temperatures in any TPD technique due to the kinetics of desorption this agrees reasonably well with the decomposition temperature of $YONO_3$ to Y_2O_3 of 450°C (34). The two desorption peaks observed between 200 and 350°C may be associated with the decomposition of the nitrite and bidentate nitrate species identified via DRIFT, while the major peak at 420°C is likely due to decomposition of unidentate nitrate species.

Quantification of weakly chemisorbed NO_x species on Y_2O_3 was performed in order to determine the degree of reversible adsorption at elevated temperatures. Surface adsorption of NO_x in the presence of gas-phase NO and O_2 on Y1000 was determined by thermal gravimetric analysis (TGA) (Fig. 4). This study reveals that there is a reversible adsorption of NO_x on the catalyst surface above 500°C, and that the quantity adsorbed steadily decreases with temperature. At temperatures in excess of 800°C, there is very little surface adsorption of NO_x species.

In situ DRIFT studies of Y600 were performed in order to identify whether any intermediate reaction species could be detected on the surface of a working catalyst. A DRIFT spectrum of Y600 exposed to NO, CH_4, and O_2 at 500°C is shown in Fig. 5. Strong peaks due to adsorbed hydroxyl species (3650–3400 cm^{-1}), gas-phase CH_4 (3016 cm^{-1}, 1305 cm^{-1}), gas-phase CO_2 (2362 cm^{-1}, 2331 cm^{-1}), and adsorbed carbonates and nitrates (1650–1100 cm^{-1}) (35) are evident in the spectrum. A weak feature at 2176 cm^{-1} is also noted. This peak was not observed when Y600 was exposed to mixtures of CH_4 and O_2 or NO and O_2 at the same temperature. Passage of CH_3NO_2 or CH_3NO over Y600 at 500°C also produced intense peaks at 2176 cm^{-1} (not shown). NCO and CN species are known to have stretching vibrations in the vicinity of 2176 cm^{-1} (19, 29, 35–37). Subsequent evacuation and NO exposure (at 500°C) of Y600 with this 2176 cm^{-1} band led to a rapid decay of the peak and the evolution of N_2 and CO_2. The presence of

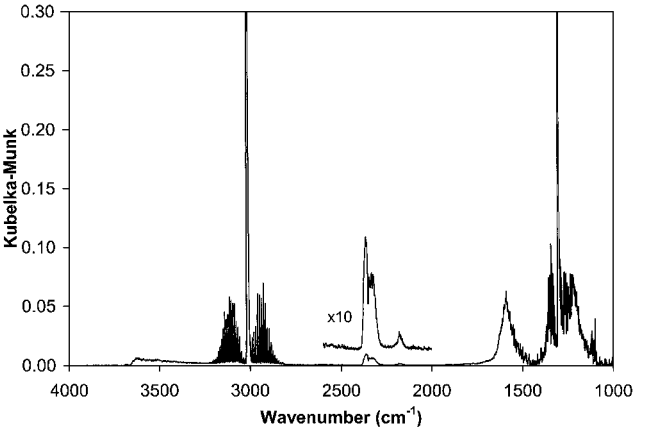

FIG. 5. DRIFT spectrum of Y600 exposed to SCR reaction mixture at 500°C.

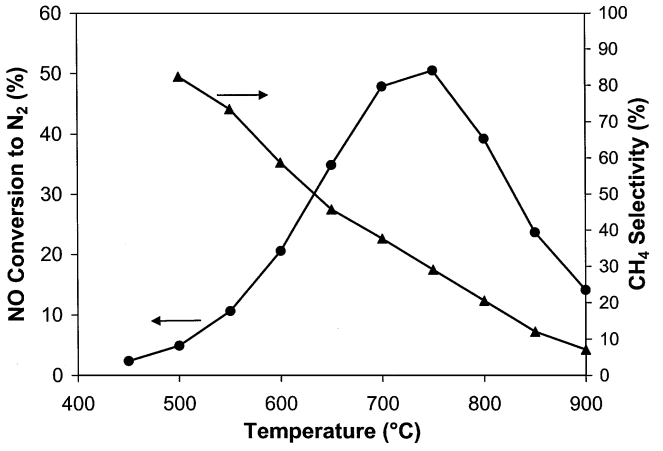

FIG. 6. The (●) NO reduction activity and (▲) CH_4 selectivity of Y1000. The reaction was run at a space velocity of 60000 h^{-1} with 4000 ppm NO, 4000 ppm CH_4, and 8000 ppm O_2.

CO_2 in the effluent suggests that the adsorbed species is NCO, rather than CN. Thus, C–N coupling appears to be a critical step in the reduction of NO_x with CH_4, and any mechanism proposed for the reduction of NO_x over Y_2O_3 must account for the formation of NCO intermediates.

The high-temperature activity of Y1000 is shown in Fig. 6. It reveals that the steady loss of CH_4 selectivity observed in Fig. 1b continues to at least 900°C, where an overall NO conversion of 14% is noted. The presence of activity at temperatures in excess of those where significant NO_x adsorption occurs (Fig. 4) suggests that surface reaction of CH_3 species with adsorbed NO_x is not required for SCR activity. Coupling of CH_3 radicals with NO_x species in the gas phase appears to be a likely route for C–N bond formation at 900°C. The absence of any abrupt change in CH_4 selectivity from 900 to 500°C may also suggest that there is no transition to a surface coupling reaction as the temperature decreases.

Previous studies of methane oxidative coupling catalysts for the SCR of NO_x with CH_4 have noted a lack of C2 product generation in the presence of NO, and they have thus suggested that surface-generated methyl species react with NO_x on the catalyst surface before they can desorb into the gas phase (9). We have, in fact, detected ethane and ethene in the effluent from a Y800 catalyst under SCR conditions. Figure 7 shows the amounts of C_2H_6 and C_2H_4 produced upon exposure of Y800 to 2% CH_4, 5% O_2, and variable amounts of NO at 700°C. There is a gradual decrease in the amount of coupling products as NO is added to the system. The formation of these species in the presence of 7100 ppm NO further supports the proposition that, under SCR conditions, CH_3 radicals desorb from the catalyst surface and undergo reactions in the gas phase. The reason for the decrease in coupling products will be discussed later in this article.

Once CH_3 radicals desorb into the gas phase, homogeneous reaction kinetics will determine through which pathways CH_3 radicals are ultimately converted into CO_x and H_2O. The predominant gas-phase species present under SCR conditions are O_2, CH_4, NO, NO_2, CO, CO_2, and H_2O. Several radical species, such as CH_3 and OH, will also be present, but at low concentrations, because of their short lifetimes. Separate measurements of NO oxidation over Y_2O_3 indicate that gas-phase equilibrium distributions of NO, NO_2, and O_2 are very rapidly established over Y_2O_3 at temperatures above 500°C. This, coupled with kinetic data for elementary reactions of CH_3 with O_2 (38), NO (38), NO_2 (39), and CH_3 (38), allows one to predict the dominant pathways through which CH_3 radicals will be consumed in the gas phase.

$$CH_3 + O_2 \rightarrow CH_3O_2 \quad [R1a]$$

$$CH_3 + O_2 \rightarrow CH_3O + O \quad [R1b]$$

$$CH_3 + O_2 \rightarrow CH_2O + OH \quad [R1c]$$

$$CH_3 + NO \rightarrow CH_3NO \quad [R2]$$

$$CH_3 + NO_2 \rightarrow CH_3NO_2 \quad [R3a]$$

$$CH_3 + NO_2 \rightarrow CH_3O + NO \quad [R3b]$$

$$CH_3 + CH_3 \rightarrow C_2H_6 \quad [R4]$$

Table 2 presents published rate expressions for homogeneous reactions of CH_3, the corresponding rate constant at 600°C, and the homogeneous rate of reaction at 600°C given a feed of 4000 ppm NO, 4000 ppm CH_4, and 4% O_2. The rate constant for CH_3 coupling [R4] is at its high pressure limit at 600°C and 1 atm (40), but because of the fewer vibrational modes in CH_3O_2 and CH_3NO, [R1a] and [R2] are in the fall-off regime under these conditions (41, 42). Pressure dependencies for [R3a] have not been reported. We have chosen to employ the high pressure limiting rate constants

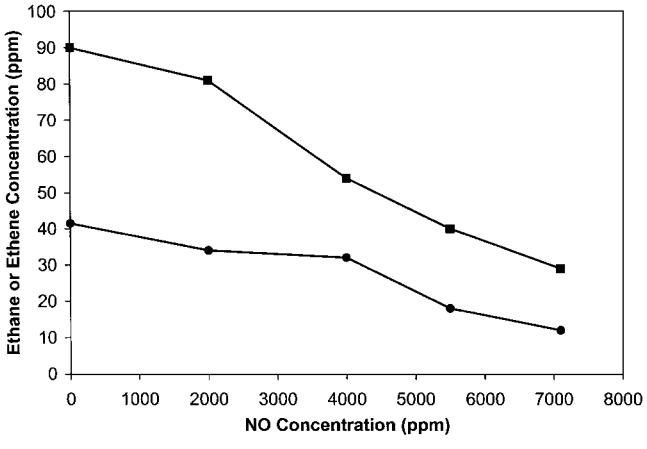

FIG. 7. Effect of NO concentration on (■) ethane and (●) ethene production over Y800 at 700°C. The reaction was run at a space velocity of 270000 h^{-1} with 2% CH_4, 5% O_2, and varying NO concentration.

TABLE 2

Homogeneous Reaction Kinetics at 600°C of Interest for SCR of NO_x with CH_4

Reaction	Rate expression	Rate constant ($cm^3/mol \cdot s$)	Rate[a] ($mol/cm^3 \cdot s$)	Ref.
[R1a]	$7.80 \times 10^8\ (T)^{1.2}$	2.64×10^{12}	$1.47 \times 10^6\ [CH_3]$	(38)
[R1b]	$1.32 \times 10^{14} \exp(-15803/T)$	1.82×10^6	$1.02 \times 10^0\ [CH_3]$	(38)
[R1c]	$3.31 \times 10^{11} \exp(-4500/T)$	1.91×10^9	$1.07 \times 10^3\ [CH_3]$	(38)
[R2]	$2.20 \times 10^{11}\ (T)^{0.6}$	1.28×10^{13}	$6.70 \times 10^5\ [CH_3]$	(38)
[R3a]	$1.00 \times 10^{13}\ (T/1000)^{-0.6}$	1.08×10^{13}	$3.75 \times 10^4\ [CH_3]$	(39)
[R3b]	1.39×10^{13}	1.39×10^{13}	$4.80 \times 10^4\ [CH_3]$	(39)
[R4]	$9.01 \times 10^{16}\ (T)^{-1.2} \exp(-329/T)$	1.83×10^{13}	$1.83 \times 10^{13}\ [CH_3]^2$	(38)

[a] Based on a feed stream containing 4000 ppm NO (3752 ppm NO and 248 ppm NO_2 at equilibrium), 4000 ppm CH_4, and 4% O_2.

for the association reactions [R1a, R2, R3a, R4] because of the additional collisional stabilization that is provided by the catalyst surface over the purely homogeneous case.

The kinetic theory of gases can be used to estimate the relative frequency of heterogeneous and homogeneous collisions of the energized adducts produced in [R1a, R2, and R3a] (43, 44). For instance, the gas-phase collision frequency of a molecule of CH_3NO in a mixture of 3752 ppm NO, 248 ppm NO_2, 4000 ppm CH_4, 4% O_2, and 95.2% He is $6.8 \times 10^9\ s^{-1}$ at 600°C (employing molecular diameters of 3.654 Å for NO (approximated as CO), 3.763 Å for NO_2 (approximated as CO_2), 3.75 Å for CH_4, 3.458 Å for O_2, 2.581 Å for He (45), and 4.25 Å for CH_3NO (46)). The surface collision frequency of CH_3NO with Y800 (surface area = 50 m^2/g, pore volume = $7.6 \times 10^{-7}\ m^3/g$) at 600°C is calculated to be $1.1 \times 10^{10}\ s^{-1}$. This is over 50% greater than the gas-phase collision frequency.

Gas–surface collisions have also been shown to be an order of magnitude more efficient at vibrational energy transfer than collisions with common bath-gas molecules (45, 47–49). Gas–surface collisions such as those between excited NO molecules and an LiF surface at 627°C have been calculated to involve an energy transfer of 7 kJ/mol (50), while collisions between cyclobutene and a silica surface between 527 and 602°C were estimated to transfer 13–49 kJ/mol (48, 49). The average energy transferred from energized species in gas-phase collisions with He and N_2 has been determined to be 0.9–1.8 kJ/mol and 2.4–3.8 kJ/mol, respectively (41, 45, 51). Although the complexity of the deactivating molecule and the frequencies of the vibrational modes of the surface play a large role in determining the collisional energy transfer, we expect that the presence of a heterogeneous catalyst will definitely result in an enhancement of the collisional stabilization of bimolecular adducts.

The reaction rates presented in Table 2 indicate that the gas-phase coupling of CH_3 with NO [R2] is favored over the coupling with NO_2 [R3a]. This is primarily due to the low equilibrium concentration of NO_2 (248 ppm) in the gas phase. Furthermore, one sees that the rate of reaction of CH_3 with O_2 [R1a] is only about twice that of the coupling of CH_3 with NO [R2], despite the presence of ten times more O_2 in the feed stream than NO. Thus, the source of selectivity in the presence of excess O_2 is demonstrated. The published rate expressions for [R1a] and [R2] indicate that [R1a] is a much stronger function of temperature than [R2] (38). The shift in consumption of CH_3 radicals via [R1a] rather than [R2] predicted by the homogeneous mechanism as the temperature increases may be the source of the steady decrease in CH_4 selectivity observed in Figs. 1b and 6.

In addition to the homogeneous reactions of CH_3 with O_2 and NO_x, the loss of CH_3 on the surface of the catalyst undoubtedly plays an important role in the overall consumption pathway of CH_3 radicals.

$$CH_3 + O* \rightarrow CO_x + H_2O \qquad [R5]$$

By temporarily excluding this heterogeneous reaction from our consideration of CH_3 consumption pathways, we can calculate a maximum CH_4 selectivity based on the homogeneous reactions of CH_3 with O_2, NO, and NO_2. The maximum selectivity can be calculated as

$$\text{Selectivity} = (\text{rate of reactions R2, R3a})/(\text{rate of reactions R1a, R1b, R1c, R2, R3a, R3b}).$$

[R2] and [R3a] are assumed to be the only selective reactions, as they are the only reactions that lead to C–N bond formation. Reactions that lead to the formation of methylperoxy [R1a], methoxy [R1b, R3b], and CH_2O [R1c] species are assumed to be nonselective, as rapid pathways to CO_x and H_2O exist for these intermediates (38). An accurate assessment of the CH_3 radical concentration is required to include the formation of C2 coupling products [R4] as a nonselective CH_3 consumption pathway. However, given the low CH_4 concentration (4000 ppm) used in this study, [R4] is likely an insignificant reaction. In fact, a concentration of several hundred ppm CH_3 is required to produce a reaction rate for [R4] comparable to that of [R3a] or [R3b],

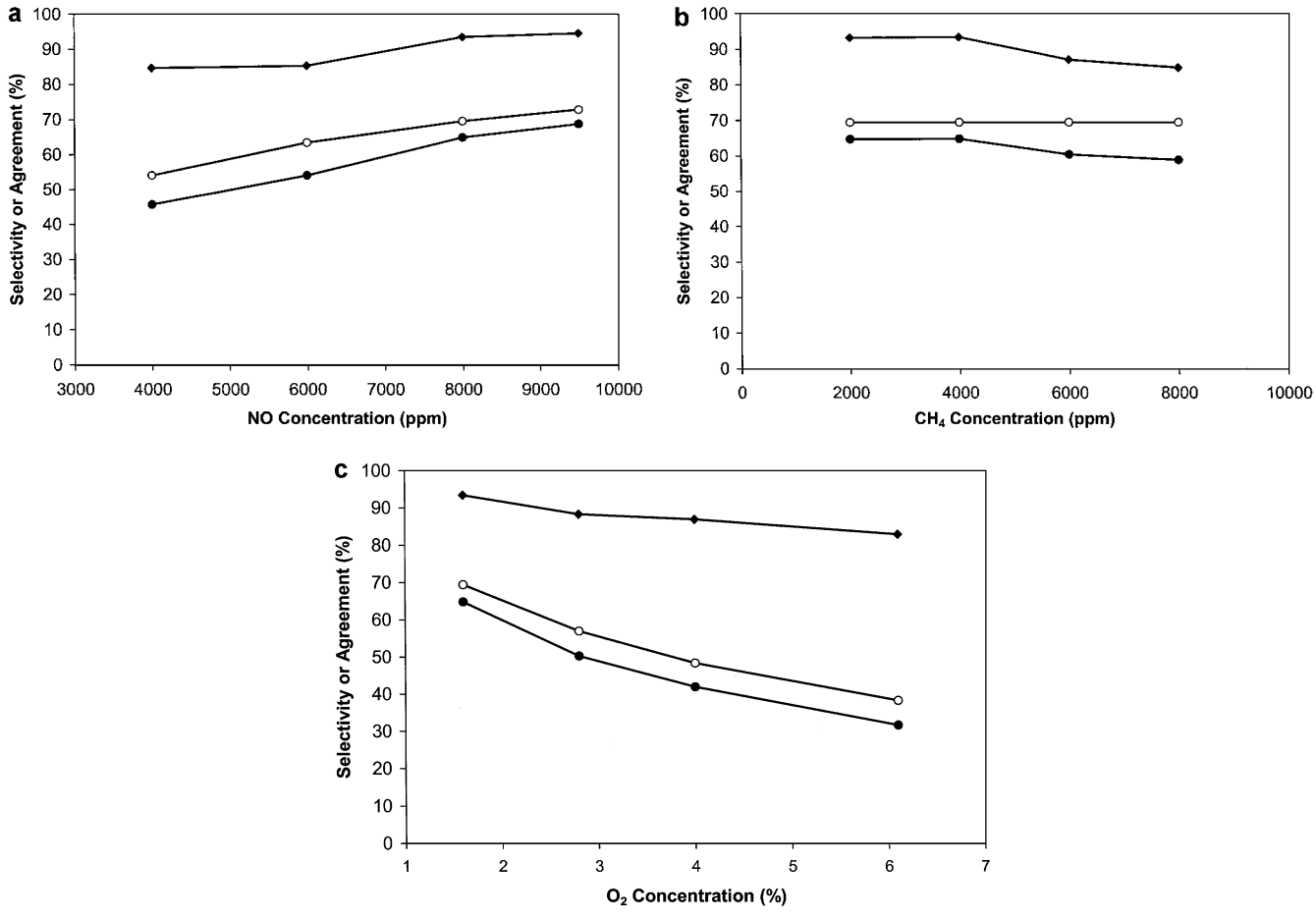

FIG. 8. (○) Predicted CH_4 selectivity, (●) measured CH_4 selectivity, and (◆) agreement between predicted and measured values, over Y800 at 600°C as a function of (a) NO concentration with 4000 ppm CH_4 and 1.6% O_2, (b) CH_4 concentration with 8000 ppm NO and 1.6% O_2, and (c) O_2 concentration with 8000 ppm NO and 4000 ppm CH_4. The reaction was run at a space velocity of 270000 h^{-1}.

which themselves are minor reaction pathways. Any nonselective heterogeneous reactions of CH_3 via [R5] will result in a lower CH_4 selectivity than predicted.

The CH_4 selectivities measured over Y800 at 600°C under differential reactor operating conditions were compared to selectivities predicted by this homogeneous reaction mechanism. Predicted and measured selectivities are shown in Fig. 8 as a function of different feed compositions. The agreement between the homogeneous selectivity limit and the experimental values is excellent, with the measured values being approximately 85–95% of those predicted by homogeneous kinetics. Small differences in the measured and predicted values as a function of concentration can primarily be attributed to the heterogeneous reaction of CH_3 radicals with surface oxygen species [R5]. The agreement between predicted and measured selectivities decreases with increasing O_2 pressure (Fig. 8c). At the higher O_2 pressure, more oxygen is expected to be present on the catalyst surface, and the heterogeneous reaction becomes more important relative to reactions [R2] and [R3a]. Similarly, the agreement between predicted and measured values as a function of NO pressure increases as P_{NO} increases (Fig. 8a), as the significance of reaction [R5] relative to reactions [R2] and [R3a] decreases. The decrease in agreement as P_{CH_4} increases (Fig. 8b) may possibly be due to the increased likelihood of CH_3 coupling to form C_2H_6 [R4], which may be a nonselective pathway for CH_3 consumption.

The decrease in coupling products observed upon addition of NO to the feed stream (Fig. 7) can also be explained by this homogenous reaction pathway. Under methane oxidative coupling conditions, the amount of C2 products generated is governed by the rate of CH_3 radical coupling [R4] versus the oxidation of CH_3 radicals [R1]. Addition of NO to the gas stream results in additional pathways [R2, R3] for CH_3 radical consumption, and hence less coupling to form C_2H_6. An estimation of the effect that NO should have on C2 production can be made by calculating what we call an "equivalent oxygen concentration" from our homogeneous reaction mechanism. This "equivalent oxygen concentration" is defined as the concentration of oxygen that produces a CH_3 consumption rate (via [R1]) equivalent

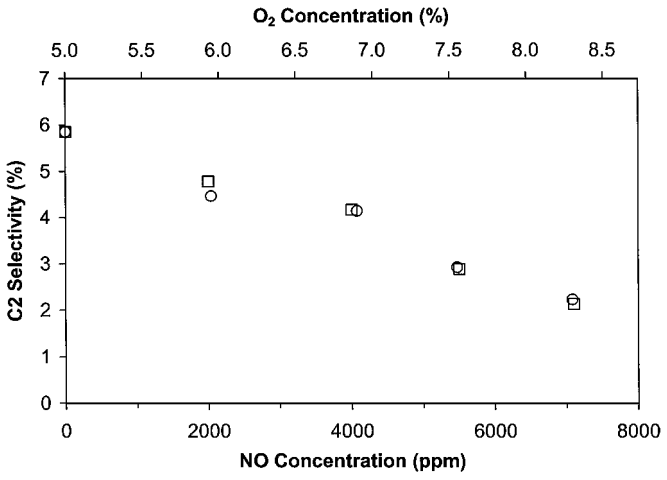

FIG. 9. Selectivity to ethane and ethene production over Y800 at 700°C as a function of (○) O_2 concentration with 2% CH_4 and (□) NO concentration with 2% CH_4 and 5% O_2. The reaction was run at a space velocity of 270000 h^{-1}.

to the total consumption rate (through [R1, R2, and R3]) when NO is present. For example, because the reaction rate constant for [R1a] is approximately 4 or 5 times less than the rate constants for [R2] or [R3], the addition of 0.2% NO to a stream containing CH_4 and O_2 would be equivalent to the addition of 0.8 to 1.0% O_2 (exact value from model: 0.95%) to the same stream. The selectivity to C2 products in each case should be the same, because the selective and nonselective CH_3 consumption rates remain unchanged. Figure 9 presents C2 selectivity for Y800 measured as a function of NO concentration in the presence of 2% CH_4 and 5% O_2 (lower ordinate), and as a function of O_2 concentration in the presence of 2% CH_4 (upper ordinate). The two ordinate axes are scaled so that the O_2 concentration, presented on the upper axis, corresponds to the "equivalent O_2 concentration" for the given amount of NO with 5% O_2, presented on the lower axis. It is evident that the homogeneous reaction mechanism does an excellent job describing the coupling behavior of this system. Again, heterogeneous reactions are not accounted for, but if the catalyst does not significantly oxidize CH_3 radicals (Fig. 8), oxidation of coupling products will also not be severe.

In addition to the prediction of CH_3NO as the reaction intermediate through homogeneous modeling, catalytic studies have also been used to confirm the importance of CH_3NO over CH_3NO_2. We have performed catalytic studies on reactions of CH_3NO_2 and CH_3NO with NO and O_2 over Y_2O_3, and examined the efficiency of N_2 and N_2O production from the different intermediates. Approximately 800 ppm CH_3NO_2 or CH_3NO, 4000 ppm NO, and 8000 ppm O_2 were passed over Y600 at 600°C. Complete reaction of both CH_3NO_x species occurred, with the primary products detected by gas chromatography being CO_2, N_2O, and N_2. Table 3 lists the product distributions from each reaction and the selectivity of N_2 and N_2O production from CH_3NO_2 and CH_3NO (selectivity = (N_2 and N_2O produced)/(CO_x generated)). The CH_3NO molecule efficiently reacts with NO_x to produce N_2 and N_2O, while only two-thirds of the CH_3NO_2 molecules react with NO_x to form N_2 or N_2O under the same conditions. Lombardo *et al.* observed similar selectivities (55–80%) for CH_3NO_2 reactions with NO and O_2 over Co-, H-, Fe-, and Cu-ZSM-5 at 600°C (17). Also shown in Table 3 are the product distribution and methane selectivity of the same catalyst exposed to a reaction mixture containing 4000 ppm NO, 4000 ppm CH_4, and 8000 ppm O_2 at space velocities of 60000 and 100000 h^{-1}. Regardless of the CH_4 conversion, the selectivity for N_2 and N_2O production from methane (which includes the nonselective oxidation of CH_3 species) in SCR is greater than that observed when CH_3NO_2 is passed over the catalyst. Thus, CH_3NO_2 is definitely not the intermediate species that is responsible for N_2 production under SCR reaction conditions.

A possible mechanism for N_2 formation from CH_3NO, based on published homogeneous reactions, is as follows.

$$CH_3 + NO \rightarrow CH_3NO \quad [R6]$$

$$CH_3NO \rightarrow CH_2NOH \quad [R7]$$

$$CH_2NOH \rightarrow HCN + H_2O \quad [R8]$$

$$HCN + O \rightarrow CN + OH \quad [R9]$$

$$HCN + O \rightarrow NCO + H \quad [R10]$$

$$HCN + OH \rightarrow CN + H_2O \quad [R11]$$

$$CN + O_2 \rightarrow NCO + O \quad [R12]$$

$$CN + OH \rightarrow NCO + H \quad [R13]$$

$$NCO + NO \rightarrow N_2O + CO \quad [R14]$$

$$NCO + NO \rightarrow N_2 + CO_2 \quad [R15]$$

$$CN + NO \rightarrow N_2 + CO \quad [R16]$$

$$N_2O \rightarrow N_2 + O \quad [R17]$$

TABLE 3

Product Distributions over Y600 for Reactions of CH_3NO_2, CH_3NO, and CH_4 at 600°C

Reactant	CO_2 (ppm)	CO (ppm)	N_2 (ppm)	N_2O (ppm)	Selectivity (%)
CH_3NO_2[a]	893	0	458	144	67
CH_3NO[a]	596	0	498	87	98
CH_4[b]	1153	131	809	72	69
CH_4[c]	663	69	452	53	69

[a] Feed stream consists of approximately 800 ppm CH_3NO_x, 4000 ppm NO, and 8000 ppm O_2 (GHSV = 60000 h^{-1}).

[b] Feed stream consists of 4000 ppm CH_4, 4000 ppm NO, and 8000 ppm O_2 (GHSV = 60000 h^{-1}).

[c] Feed stream consists of 4000 ppm CH_4, 4000 ppm NO, and 8000 ppm O_2 (GHSV = 100000 h^{-1}).

We do not propose that these reactions occur solely in the gas phase but rather we are using these homogeneous reactions to describe what may occur on the catalyst surface. The isomerization of nitrosomethane to formaldoxime [R7] readily occurs in the gas phase and has been observed to proceed at temperatures as low as 230°C (52). However, published homogeneous rate constants for [R7] do not allow for full gas-phase conversion of nitrosomethane to formaldoxime within the residence time of our reactor. Density functional theory calculations indicate that transition metal cations can catalyze the 1,3-hydrogen shift (or two successive 1,2-hydrogen shifts) involved in the isomerization of nitrosomethane to formaldoxime; 1,3-hydrogen shifts are also readily catalyzed by basic catalysts, so it is likely that [R7] is a heterogeneous reaction (53–55).

Saito *et al.* have studied the thermal reactions of formaldoxime at high temperatures and have observed HCN and H_2O as the primary decomposition products [R8] (56). They observed negligible reisomerization of fomaldoxime to CH_3NO and negligible decomposition of formaldoxime to H_2CN and OH. We have detected small amounts of HCN in the reactor effluent when operating under excess CH_4 ($CH_4/O_2 = 2:1$), but under SCR conditions (i.e., excess O_2), no HCN has been detected. The rapid oxidation of HCN to NCO and CN described in [R9] through [R13] accounts for this observation (57, 58).

The final step involves the conversion of NCO and CN species to molecular nitrogen and CO_x. Between room temperature and 300°C, measurements of the homogeneous reaction of NCO and NO indicate that N_2 and CO_2 [R15] are preferentially formed over N_2O and CO [R14] (59). We have also observed the conversion of surface adsorbed NCO to N_2 and CO_2 at 500°C in our DRIFT studies. Reaction [R14] was also proposed by Vannice *et al.* to play a role in the SCR of NO_x with methane over La_2O_3 and Sr/La_2O_3 (22), and a reaction similar to [R16] has been proposed to play a role in the SCR of NO_x over Co-ZSM-5 (29). The presence of N_2O in the effluent from Group IIIB metal oxide catalysts likely arises from [R14], but at elevated temperatures (≥600°C), the decomposition of nitrous oxide to nitrogen and oxygen readily proceeds over these high surface area oxide catalysts, and little N_2O is observed in the exhaust stream (10).

CONCLUSIONS

A heterogeneous/homogeneous reaction mechanism is proposed to explain the high catalytic activities observed for the SCR of NO_x with methane over yttrium oxide. The reaction is initiated by the surface generation of CH_3 radicals from CH_4, as is the case for methane oxidative coupling. This is followed by gas-phase formation of reactive intermediates and subsequent heterogeneous transformation of these intermediates to N_2, CO, CO_2, and H_2O.

Predictions of CH_4 selectivity based on a homogeneous reaction model for the consumption of CH_3 radicals through reactions with O_2, NO, and NO_2 are in very good agreement with experimentally determined values. Both the homogeneous reaction model and an examination of catalytic reactions of possible intermediates indicate that nitrosomethane is the key reaction intermediate in the SCR of NO_x with methane over yttrium oxide. Reaction of nitrosomethane to N_2 occurs with a very high selectivity through a series of heterogeneous reactions that involve CH_2NOH, CN, NCO, and N_2O as further intermediates.

ACKNOWLEDGMENTS

The authors thank Eugene Chiu for his assistance with the synthesis of the nanocrystalline catalysts, as well as Michael S. Wong for his help with the DRIFT studies. This work was supported by the National Science Foundation (CTS-9731396).

REFERENCES

1. Armor, J. N., *Appl. Catal. B Env.* **1**, 221 (1992).
2. Shelef, M., *Chem. Rev.* **95**, 209 (1995).
3. Armor, J. N., *Catal. Today* **26**, 147 (1995).
4. Li, Y., and Armor, J. N., *Appl. Catal. B Env.* **1**, L31 (1992).
5. Li, Y., and Armor, J. N., *Appl. Catal. B Env.* **2**, 239 (1993).
6. Li, Y., and Armor, J. N., *Appl. Catal. B Env.* **3**, L1 (1993).
7. Zhang, X., Walters, A. B., and Vannice, M. A., *J. Catal.* **155**, 290 (1995).
8. Otsuka, K., Zhang, Q., Yamanaka, I., Tono, H., Hatano, M., and Kinoshita, H., *Bull. Chem. Soc. Jpn.* **69**, 3367 (1996).
9. Zhang, X., Walters, A. B., and Vannice, M. A., *J. Catal.* **146**, 568 (1994).
10. Fokema, M. D., and Ying, J. Y., *Appl. Catal. B Env.* **18**, 71 (1998).
11. Teraoka, Y., Haruda, T., Iwasaki, T., Ikeda, T., and Kagawa, S., *Chem. Lett.*, 773 (1993).
12. Feeley, J. S., Deeba, M., Farrauto, R. J., Beri, G., and Haynes, A., *Appl. Catal. B Env.* **6**, 79 (1995).
13. Shimizu, K., Satsuma, A., and Hattori, T., *Appl. Catal. B Env.* **16**, 319 (1998).
14. Li, Y., and Armor, J. N., *J. Catal.* **150**, 376 (1994).
15. Cowan, A. D., Dümpelmann, R., and Cant, N. W., *J. Catal.* **151**, 356 (1995).
16. Cant, N. W., Cowan, A. D., Doughty, A., Haynes, B. S., and Nelson, P. F., *Catal. Lett.* **46**, 207 (1997).
17. Lombardo, E. A., Sill, G. A., d'Itri, J. L., and Hall, W. K., *J. Catal.* **173**, 440 (1998).
18. Sun, T., Fokema, M. D., and Ying, J. Y., *Catal. Today* **33**, 251 (1997).
19. Lobree, L. J., Aylor, A. W., Reimer, J. A., and Bell, A. T., *J. Catal.* **169**, 188 (1997).
20. Sun, T., Trudeau, M. L., and Ying, J. Y., *J. Phys. Chem.* **100**, 13662 (1996).
21. Budi, P., and Howe, R. F., *Catal. Today* **38**, 175 (1997).
22. Vannice, M. A., Walters, A. B., and Zhang, X., *J. Catal.* **159**, 119 (1996).
23. Xie, S., Ballinger, T. H., Rosynek, M. P., and Lunsford, J. H., *in* "Proceedings, 11th International Congress on Catalysis, 40th Anniversary" (J. W. Hightower, W. N. Delgass, E. Iglesia, and A. T. Bell, Eds.), p. 711. Elsevier, Amsterdam, 1996.
24. Lunsford, J. H., *in* "Methane Conversion by Oxidative Processes: Fundamental and Engineering Aspects" (E. E. Wolf, Ed.), p. 3. Van Nostrand–Reinhold, New York, 1992.
25. Maitra, A. M., Campbell, I., and Tyler, R. J., *Appl. Catal. A Gen.* **85**, 27 (1992).
26. Fokema, M. D., and Ying, J. Y., submitted.

27. Fokema, M. D., Chiu, E., and Ying, J. Y., *Langmuir*, in press.
28. Coe, C. S., and Doumani, T. F., *J. Am. Chem. Soc.* **70**, 1516 (1948).
29. Aylor, A. W., Lobree, L. J., Reimer, J. A., and Bell, A. T., *in* "Proceedings, 11th International Congress on Catalysis, 40th Anniversary" (J. W. Hightower, W. N. Delgass, E. Iglesia, and A. T. Bell, Eds.), p. 661. Elsevier, Amsterdam, 1996.
30. Davydov, A. A., Lokhov, Y. A., and Shchekochokhin, Y. M., *Kinet. Katal.* **19**, 673 (1978).
31. Bodenstein, M., *Z. Phys. Chem.* **100**, 68 (1922).
32. Pozdnyakov, D. V., and Filimonov, V. N., *Kinet. Katal.* **14**, 760 (1971).
33. Klingenberg, B., and Vannice, M. A., *Chem. Mater.* **8**, 2755 (1996).
34. Pelloquin, D., Louër, M., and Louër, D., *J. Solid State Chem.* **112**, 182 (1994).
35. Nakamoto, K., "Infrared Spectra of Inorganic and Coordination Compounds." Wiley, New York, 1978.
36. Ukisu, Y., Sato, S., Abe, A., and Yoshida, K., *Appl. Catal. B Env.* **2**, 147 (1993).
37. Solymosi, F., and Bansagi, T., *J. Catal.* **156**, 75 (1995).
38. Bromly, J. H., Barnes, F. J., Muris, S., You, X., and Haynes, B. S., *Combust. Sci. Technol.* **115**, 259 (1996).
39. Glänzer, K., and Troe, J., *Ber. Bunsen. Phys. Chem.* **78**, 182 (1974).
40. Dean, A. M., *J. Phys. Chem.* **89**, 4600 (1985).
41. Keiffer, M., Pilling, M. J., and Smith, M. J. C., *J. Phys. Chem.* **91**, 6028 (1987).
42. Wolff, T., and Wagner, H. G., *Ber. Bunsen. Phys. Chem.* **92**, 678 (1988).
43. Glasstone, S., Laidler, K. J., and Eyring, H., "The Theory of Rate Processes." McGraw–Hill, New York, 1941.
44. Laidler, K. J., "Chemical Kinetics." Harper Collins, New York, 1987.
45. Dean, A. M., Bozzelli, J. W., and Ritter, E. R., *Combust. Sci. Technol.* **80**, 63 (1991).
46. Bozzelli, J. W., and Dean, A. M., *in* "Combustion Chemistry," (W. C. Gardiner, Jr., Ed.) 2nd ed. Springer-Verlag, New York, 1994.
47. Golden, D. M., Spokes, G. N., and Benson, S. W., *Angew. Chem. Int. Ed.* **12**, 534 (1973).
48. Yuan, W., and Rabinovitch, B. S., *J. Chem. Phys.* **80**, 1687 (1984).
49. Kelley, D. F., Kasai, T., and Rabinovitch, B. S., *J. Phys. Chem.* **85**, 1100 (1981).
50. Lucchese, R. R., and Tully, J. C., *J. Chem. Phys.* **80**, 3451 (1984).
51. Hippler, H., Lindemann, L., and Troe, J., *J. Chem. Phys.* **83**, 3906 (1985).
52. Batt, L., and Gowenlock, B. G., *Trans. Faraday Soc.* **56**, 682 (1960).
53. Vladimiroff, T., *J. Mol. Struct.* **410**, 141 (1997).
54. Alcamí, M., Mó, O., Yáñez, M., Luna, A., Morizur, J.-P., and Tortajada, J., *J. Phys. Chem. A* **102**, 10120 (1998).
55. Arai, T., Tobita, S., and Shizuki, H., *J. Am. Chem. Soc.* **117**, 3968 (1995).
56. Saito, K., Makishita, K., Kakumoto, T., Sasaki, T., and Imamura, A., *J. Phys. Chem.* **92**, 4371 (1988).
57. Higashihara, T., Saito, K., and Murakami, I., *J. Phys. Chem.* **87**, 3707 (1983).
58. Glarborg, P., and Miller, J. A., *Combust. Flame* **99**, 475 (1994).
59. Cooper, W. F., Park, J., and Hershberger, J. F., *J. Phys. Chem.* **97**, 3283 (1993).